

pubs.acs.org/JPCA Article

Functionalized Ferrocene Enables Selective Electrosorption of Arsenic Oxyanions over Phosphate—A DFT Examination of the Effects of Substitutional Moieties, pH, and Oxidation State

Obinna Nwokonkwo, Vivienne Pelletier, Michael Broud, and Christopher Muhich*



Cite This: J. Phys. Chem. A 2023, 127, 7727-7738



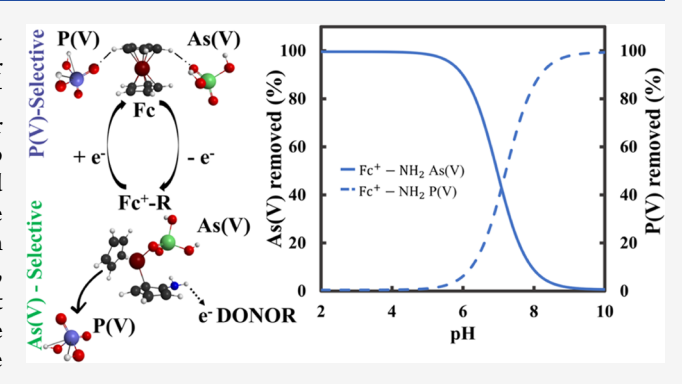
ACCESS I

III Metrics & More

Article Recommendations

s Supporting Information

ABSTRACT: Ferrocene (Fc)/ferrocenium (Fc⁺)-decorated carbon nanotube electrode materials have shown promise for selectively adsorbing arsenic (As) over dissimilar anions like Cl⁻ and ClO₄⁻, and isostructural transition-metal oxyanions for water remediation; however, the competition between same-group oxyanions (such as arsenate vs phosphate) is underexplored and poorly understood. We use *ab initio* calculations to examine the competitive binding of As(V), P(V), and As(III) to Fc/Fc⁺ with and without functional substitutions (OH, SH, NH₂, COOH, CH₃, C₂H₅, NO₂, and Cl). This work aims to understand factors that induce the selective binding of toxic arsenic over phosphate. We find that neat Fc cannot distinguish the three oxyanions because physical forces (electrostatics and dispersion) dominate the Fc-



oxyanion interactions. However, combined oxidation and substitution effects enable selectivity for As(V) over P(V). Oxidation of Fc to Fc⁺ allows the formation of Fc⁺-oxyanion covalent bonds with varying donor—acceptor character depending on the oxyanion. Additionally, NH_2 and SH groups that donate charge to the base Fc^+ molecule and H-bond to oxyanion induce an energetic preference for As(V) over P(V) by -0.23 and -0.13 eV, respectively. Differences in pK_a between As(V)/P(V) and As(III) preclude any preference for As(III) over the other anions. Using the calculated energetics, we predict the pH-dependent binding selectivity of functionalized ferrocenium. These findings demonstrate the challenges of Fc/Fc^+ -oxyanion interaction for selective binding and provide a path for identifying other molecules and substituents for efficient metallocene adsorbent design.

1. INTRODUCTION

The efficient removal of arsenic (As) from drinking water remains a pressing engineering and environmental challenge in distributed drinking water systems due to its severe toxicity even at low levels. Ingestion of As causes cancer, liver, kidney, and lung deterioration, ulcers, and neurodegenerative disorders. Therefore, the World Health Organization (WHO) recommends a maximum arsenic concentration of $10~\mu g/L$ in drinking water. Arsenic is present in aqueous environments primarily as the trivalent As(III) (arsenite) or the pentavalent As(V) (arsenate), where the protonation state is controlled by the pH given the pK_a 's of both species (6.9 and 9.2 for As(V) and As(III), respectively).

Several technologies, including precipitation, ion exchange, reverse osmosis (RO), electrodialysis, and adsorption, are deployed to remove As from water. Among these, adsorption is a promising under-the-sink remediation technology that, unlike the state-of-the-art RO systems, uses relatively inexpensive materials, requires negligible energy, and produces no secondary brine stream that must be disposed. Compared to some of the other technologies, in principle, adsorption requires no chemical input during water filtration, thus

simplifying operations for point-of-use systems. Regeneration steps may, however, require chemical treatment. In addition, conventional sorbents are relatively less susceptible to fouling and can achieve high removal efficiencies in simple water matrices containing a single toxin. However, the performance of conventional sorbents is primarily limited by the presence of less toxic competing species, such as phosphate, silicate, nitrate, sulfate, and bicarbonate, in contaminated water. These less toxic species are chemically and structurally similar to As oxyanions and often occur at higher concentrations (up to 10–100 times); thus, these oxyanions (phosphate, silicate, nitrate, sulfate, and bicarbonate) compete with As for adsorption sites on nonspecific sorbents and decrease the treated-water volume of the sorbent before replacement is necessary. Characteristics of the sorbent before replacement is necessary.

Received: June 6, 2023 Revised: August 18, 2023 Published: September 8, 2023





selectivity into sorbent materials without otherwise altering throughput or activity could decrease As concentrations in distributed drinking waters and the treatment cost.

Recently, capacitive deionization (CDI)³⁰⁻³² has attracted attention because it combines the benefits of adsorption and electrodialysis, including modularity, relative ease of operation compared to chemical treatment, and the opportunity for inducing selective separations.³¹ Additionally, CDI overcomes the challenge of handling the contaminant-saturated sorbent of conventional sorbents because of the ability to regenerate the electrodes in place. Further, CDI may resolve the issue of poor selectivity of electrodialysis by including functional electrosorbents such as redox materials that enable electrochemical ion exchange. 30,31 In CDI, polarized electrodes, commonly porous activated carbon, provide an electromotive force that drives the migration of ions toward, and adsorption to, the electrode surface, thus purifying the feed water.³³ The variable potential of the electrosorbent surface provides an additional means to externally control the sorbent-sorbate interactions beyond their innate physiochemical interactions,³⁴ and therefore can confer selectivity. Additionally, by changing the polarization direction, the ions can be repelled from the electrosorbent regenerating the surface and eliminating or substantially reducing the need to replace the sorbents.

Recent studies have examined ferrocene (Fc) tethered to carbon nanotubes as a redox-active electrosorbent for CDI. 30,31,35-39 Fc or dicyclopentadiene-Fe(II) is an inexpensive organo-metallic compound commonly used for molecular sensing, asymmetrical catalysis, biomedical applications, batteries, and others. The versatility of Fc partially arises from the relative ease in forming the oxidized ferrocenium ion (Fc+) under applied potential (0.8-1.2 V vs Ag/AgCl).⁴⁶ This feature is often exploited by incorporating Fc in host materials such as polymers, metal-organic frameworks (MOFs), and covalent-organic frameworks (COFs). Su et al. demonstrated that oxidized poly-(vinylferrocene) (PVF) coated on carbon nanotube electrodes selectively adsorbed As oxyanions over Cl⁻ and ClO₄⁻³⁷ The selective removal of As by Fc⁺ over dissimilar anions was rationalized via electrochemical, hydrogen bonding, polarizability differences, and charge transfer arguments. 36,3

Furthermore, Fc⁺ has also been shown to selectively separate isostructural heavy-metal oxyanions in complex water matrices, particularly in binary mixtures of the oxyanions.³⁴ Meanwhile, parallel work by Gani et al. on Fc/Fc⁺ binding of anions demonstrated that the inclusion of functional substitutions to the cyclopentadienyl (Cp) groups (Fc-R) can tune the selectivity of formate over perchlorate.⁴⁸ Although Fc and Fc-R exhibit preferential binding of dissimilar as well as isostructural transition-metal oxyanions, there remains a gap in mechanistic understanding of the differential binding behaviors among oxyanions particularly those in the same group of the periodic table and thus most chemically identical.

In this work, we use density functional theory (DFT) calculations to examine the competitive binding of As(V), P(V), and As(III) to Fc, Fc⁺, and their functional derivatives to determine their relative selectivity and the underlying causes. P(V) is chosen as the competing ion because it is most structurally and chemically similar to As(V). We examine As(III) as it is an As-containing molecule with different structural and electronic properties. We find that neither neat Fc nor Fc⁺ distinguishes between the three oxyanions. However, select substitutions, particularly NH₂ and SH, induce

preferential binding of As(V) over the similarly shaped P(V) molecules in the oxidized Fc^+ -R state. This work highlights the possibility of achieving preferential removal of target contaminants via tailored functional substitutions of molecular electrodes.

2. COMPUTATIONAL DETAILS

2.1. First-Principles Calculations. DFT calculations were performed using the GAUSSIAN 16 program, 50 while optimized structures were visualized using Macmolplt.⁵¹ Molecular structures were optimized at the B3LYP⁵²⁻⁵⁴ DFT level with a 6-31G+(d,p) basis set. Subsequently, binding energies were calculated with the larger aug-cc-pVTZ basis set. We calculated a maximum difference in bond length of only 0.06Å between the 6-31G+(d,p) and the much more computationally expensive aug-cc-pVTZ basis set. This procedure reduced computational costs while maintaining high energetic accuracy (see supplemental information (SI) Figure S1 for a comparison of basis sets). Van der Waals dispersion forces were accounted for via the empirical DFT D3 method of Grimme et al.⁵⁵ The B3LYP functional achieved similar binding energies and trends as MP2 calculations, having absolute deviations in binding energies and binding energy differences of less than 0.13 and 0.04 eV, respectively, compared to MP2 calculations with an aug-cc-pVTZ basis set. Therefore, the less computationally expensive B3LYP functional was used. A comparison of test set binding energies at the MP2 and B3LYP levels is shown in SI Figure S2. We examined various multiplicities for the systems and only report on the lowest-energy state for each structure: a singlet for Fc and a sextuplet for Fc+. Molecular structures were optimized until the root-mean-square gradient in structural energy was less than 0.0001 Hartree/Bohr. An implicit water solvent was implemented via the Polarizable Continuum Model (PCM)⁵⁶⁻⁵⁸ to account for solvation effects with atomic size represented using the simplified united atomic radii. We use PCM to account for solvation effects following the methods of Su et al. and Gani et al. for treating oxyanion binding to these

Binding energies for all systems were calculated using eq 1.

$$\Delta E_{\rm bind} = E_{\rm Fc+oxo} - E_{\rm Fc} - E_{\rm oxo} \tag{1}$$

where $\Delta E_{\rm bind}$ is the binding energy of the oxyanion to the Fc/Fc⁺ molecule, $E_{\rm Fc+oxo}$ is the total energy of the system with the oxyanion bound at a site on the Fc/Fc⁺ molecule, $E_{\rm Fc}$ is the total energy of isolated Fc/Fc⁺, and $E_{\rm oxo}$ is the total energy of the respective isolated oxyanion (As(V), As(III), or P(V)). A negative value for the binding energy represents an exothermic process, while a positive value corresponds to an endothermic process.

2.2. Bonding Analysis. Natural Bonding Orbital (NBO) analysis was performed using the NBO package v3.1⁵⁹ in GAUSSIAN 16. NBO calculates orbital stabilization energies and was used to quantify the extent of back-donation between Fe-O molecular orbitals in the Fc⁺—Oxyanion interaction. Furthermore, Localized Molecular Orbital-Energy Decomposition Analysis (LMO-EDA)⁶⁰ was performed in the GAMESS program.⁶¹ GAMESS was used rather than GAUSSIAN because our available implementation of GAUSSIAN did not contain the LMO-EDA capabilities. For the Fc molecule, the difference in As(V) binding energies between the GAUSSIAN and GAMESS programs was only 0.09 eV. EDA decomposes the intermolecular binding interaction between Fc/Fc⁺ and

oxyanion into electrostatic (E_s) , exchange (E_x) , electron-electron repulsion (E_{rep}) , polarization (E_{pol}) , and dispersion (E_{disp}) components.

2.3. As(V) Removal Prediction. We predict the percentage removal of As(V) on Fc/Fc^+ decorated surfaces as a function of pH using relevant equilibrium relationships. The Gibbs free energies of binding in J/mol were calculated as follows

$$\Delta G_{\text{bind}} = \Delta E_{\text{bind}} - T\Delta S - 2.3RT(pH - pK_a) \tag{2}$$

where $\Delta E_{\rm bind}$ is the electronic binding energy calculated from eq 1 in J/mol, for various As(V) and P(V) species. In the calculation of free energy, ΔS was taken as the negative of the free ion entropy in solution S_{aq} (J/mol⁻¹·K⁻¹) (taken from refs 62, 63) representing a complete loss of solution phase entropy. We performed a sensitivity analysis to determine the repercussions of this assumption on the relative removal of As(V) and P(V) by Fc⁺-NH₂. As shown in SI Figure S12, we find that the binding behavior is independent of the amount of solution phase entropy retained upon binding; in other words, we predict the same quantities of adsorption when we include no entropy loss, 50% entropy loss, and total entropy loss. Therefore, the assumption of total entropy loss does not affect any conclusion and is used for all systems considered. R is the gas constant in $(J/mol^{-1} \cdot K^{-1})$ and T is the temperature taken to be 298K, and the third term accounts for the pH-dependent oxyanion deprotonation free energy. We only calculated ΔG_{bind} for the di-protonated and mono-protonated As(V) and P(V) H₂XO₄ and HXO₄²⁻ since those are present in environmental conditions. Equilibrium binding constants were calculated

$$K = \exp\left(\frac{-\Delta G_{\text{bind}}}{RT}\right) \tag{3}$$

where K is the equilibrium constant for a given oxyanion species. Equilibrium concentrations of the two oxyanion protonation states were calculated using the pK_a values for As(V) and P(V) (6.9 and 7.2, respectively), and the relationship:

$$pK_{a} = pH + log\left(\frac{[H_{2}XO_{4}^{-}]}{[HXO_{4}^{2^{-}}]}\right)$$
(4)

To examine the competition between the As(V) and P(V) species, the fractional occupation of the binding sites for a given As(V) species with number of protons y was estimated using eq 5.

$$\theta_{As,y} = \frac{K_{As}[H_{y}AsO_{4}^{y-3}]}{1 + K_{As,y}[H_{y}AsO_{4}^{y-3}] + K_{P,y}[H_{y}PO_{4}^{y-3}]}$$
(5)

3. RESULTS AND DISCUSSION

To understand the adsorptive selectivity of Fc and its derivatives, we used DFT to calculate the binding energies of As(V), As(III), and P(V), the closest structural analog competitor to As(V). We examined multiple binding configurations between Fc and its derivatives and the various oxyanions; we only discuss the lowest-energy configuration unless otherwise specified. We first discuss the effects of Fc oxidation state and functional substitutions on the binding of the semiprotonated states of As(V) and P(V) ($H_2AsO_4^-$ and $H_2PO_4^-$) and the fully protonated state of As(III) (H_3AsO_3)

because these are the most present species at neutral pH (\sim <7). Subsequently, we report on the effects of oxyanion protonation on binding.

3.1. As(V) Binding to Ferrocene. We calculate that As(V) binds exothermically to neutral Fc by -0.19 eV, as shown in Figure 1a. In the most favorable binding

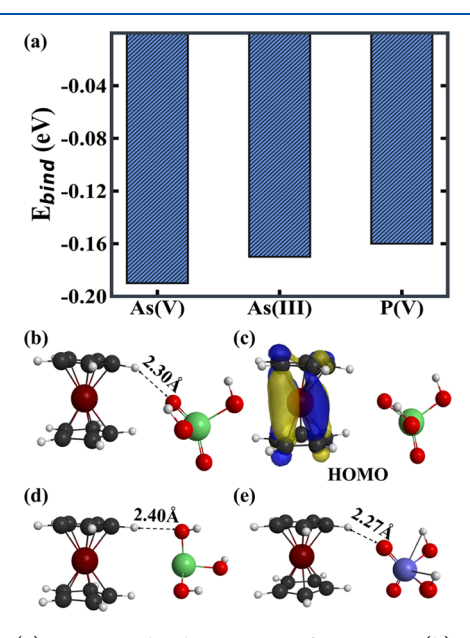


Figure 1. (a) Oxyanion binding energies for neat Fc. (b) Optimized structure for As(V) bound to Fc. (c) HOMO for As(V) bound to Fc. Optimized structures for (d) As(III) bound to Fc and (e) P(V) bound to Fc. White spheres are hydrogens, black spheres are carbon, red spheres are oxygen, purple spheres are phosphorus, dark red spheres are iron, and green spheres are arsenic.

configuration, shown in Figure 1b, As(V) binds to an H of the Cp ring by dispersion forces. Although the Fe is in a 2+ oxidation state, and thus one might assume a strong coulombic attraction between the Fe cation and As(V) anion, no direct interaction occurs because the steric repulsion of the Cp rings of Fc prevents As(V) from forming a bond to the Fe^{2+} center. This electrostatic steric repulsion also counteracts the attraction to the H of Cp, resulting in the weak binding, as revealed by EDA in Table 1. The absence of covalent bonding between Fc and As(V) is visually observed in the lack of mixing between the occupied molecular orbitals of both species, shown in Figure 1c, and the lack of significant charge transfer between Fc and As(V) upon binding (only $0.02 e^{-}$

Table 1. Localized Molecular Orbital-Energy
Decomposition Analysis (LMO-EDA) Values for the
Various Components of the Oxyanion—Fc/Fc⁺ Interactions

	Fc			Fc ⁺		
	As(V)	As(III)	P(V)	As(V)	As(III)	P(V)
E _{elect} (kcal/mol)	60.2	15.6	61.9	-68.8	-1.1	-67
$E_{\rm x}$ (kcal/mol)	-4.8	-2.8	-5.7	-51.6	-33.1	-51.1
E _{rep} (kcal/mol)	15.7	10.9	18.3	173.1	112.6	170.4
E _{pol} (kcal/mol)	-70.3	-20.6	-74	-90.8	-89.8	-91
$E_{\text{disp}} \ (\text{kcal/mol})$	-3.2	-2.9	-3.7	-12.3	-10.4	-12

from natural charge analysis), as shown in Figure S3. Thus, only dispersive forces bind As(V) to Fc. The weak interaction causes a long O···H distance of \sim 2.3 Å between Fc and As(V), which is longer than the typical H···O hydrogen bond length of \sim 1.7 Å ^{48,64} and more than double the O–H covalent bond length of \sim 0.98 Å. Overall, we predict that neutral Fc is a poor binding agent for As(V), as is seen experimentally, due to the Cp-induced steric effects, which relegate As(V)-Fc interactions to weak dispersion forces.

Fc binds As(III) and P(V) roughly equally to As(V), having binding energies of -0.17 and -0.16 eV, respectively, compared to the -0.19 of As(V). We note that all three are essentially equal within the accuracy of the computational methods used. The three oxyanions bind through weak dispersion interactions, as shown by EDA in Table 1, and the only significant difference they exhibit is the elongated bond (2.4Å) between Fc and As(III) and the slightly compressed bond (2.27 Å) for Fc-P(V), compared to As(V) (2.30 Å), as shown in Figure 1d,e, and Table 1. The bond distances for the oxyanions agree with the strength of their dispersion interactions with Fc, P(V) \geq As(V) \geq As(III). The low and essentially identical binding energies of the oxyanions imply that Fc is not only a poor binding agent but an unselective one.

3.2. As(V) Binding to Substituted Ferrocene. We investigated the influence of functional substitutions on Fcoxyanion binding strength and selectivity. We considered a series of side groups, namely, H-bond donor groups (OH, SH, NH₂, COOH), alkyl groups (CH₃ and C_2H_5), and electron-withdrawing groups (NO₂ and Cl). All groups were considered in the listed protonation state. As expected, Cl, OH, COOH, NO₂, and NH₂ withdrew charge from the core Fc structure and induced a partial positive charge on the Fc core, while SH, C_2H_5 , and CH₃ did not significantly alter the charge, as shown in Figure S4. Furthermore, the charge redistributions did not substantially alter the Fc geometric structure, shown in Figure S5.

We calculated the binding energy of As(V) at four unique sites around substituted ferrocene. Figure S4 depicts the unique sites. The increase in the number of unique sites arises from the symmetry breaking of the functional group. The groups that provide hydrogen-bonding centers (OH, COOH, NH_2 , and NO_2) increase the binding strength up to -0.64 eV (for COOH), while those that do not (CH₃, C₂H₅, and Cl) either have minimal effect or weaken binding, for example down to -0.12 eV for Fc-C₂H₅, as shown in Figure 2a. Only the lowest-energy structures for As(V) and each substituent are reported here. Table S1 reports all calculated energies. The Fc-R-As(V) intermolecular bond lengths range from 1.62Å to 1.91Å for the H-bonding groups and are consistent with typical H-bond lengths of ca. 1.7-1.9 Å. These bonds are considerably shorter than the Fc-R-As(V) bond distances of the non-Hbonding set, which range from 2.25 to 2.35 Å, as shown in Figure S6. The fact that Cl, which induced a local positive charge on Fc, did not improve As(V) binding suggests that ionic attraction is not responsible for stronger Fc-As(V) interactions. Thus, we attribute the positive effects to H-

While we attribute improved binding strength to H-bonding, we correlated the binding energy to various EDA contributions to further understand the dispersion of H-bonding within the substitution groups. EDA demonstrates that the electrostatic and dispersion components of the interaction energy were the

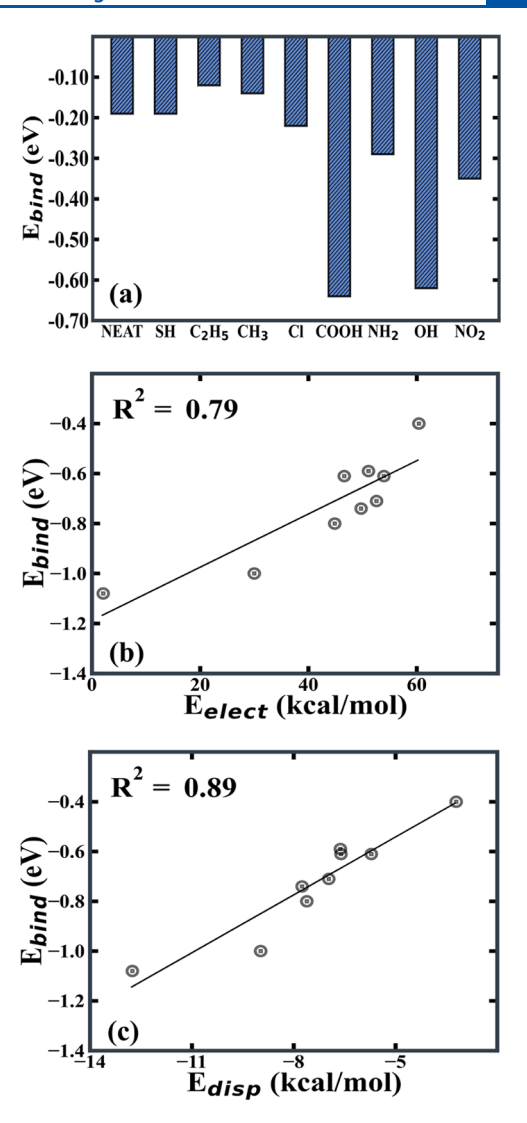


Figure 2. (a) Binding energies for As(V) bound to neat and substituted Fc. Linear correlation plots of binding energy vs (b) electrostatic component, and (c) dispersion component of the interaction between As(V) and Fc.

most correlated with binding energy with R^2 values 0.79 and 0.89, respectively, as shown in Figure 2b,c. Conversely, the interaction energy's exchange, repulsion, and polarization components had relatively weaker correlations, 0.71, 0.72, and 0.53, respectively, as shown in Figure S7. These results establish that physical interactions (dispersion and electrostatics) control As(V) binding to Fc through H-bonding and that groups with stronger H-bonding character should be sought for noncompetitive water matrices.

3.3. Substitutional Effects on As(III) and P(V) Binding. As with As(V), substitutions alter the total binding energy of As(III) and P(V) to Fc. Relative to neat Fc, binding energies were strengthened by up to $\sim 110\%$ (-0.36 eV) and $\sim 300\%$ (-0.65 eV) for As(III) and P(V), respectively, as shown in Figure 3a. We note that As(III) is in the fully protonated state, i.e., charge-neutral, as is consistent with pH ~ 7 . While As(V), As(III), and P(V) all have similar binding energies on neat Fc, the substitutions induce relative preferences of As(V) \approx P(V) \gg As (III), where the extent of preference is functional group-dependent, as shown in Figure 3b–d. Although the H-bond donating groups, i.e., NH₂, NO₂, OH, and COOH, increase

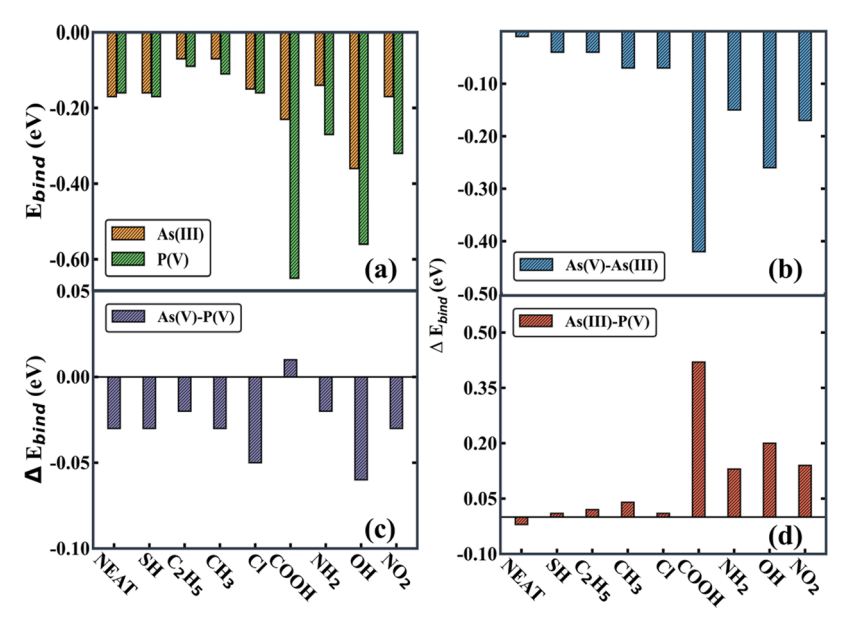


Figure 3. (a) Binding energies for As(III) and P(V) bound to neat and substituted Fc. Binding energy differences when bound to Fc between (b) As(V) and As(III), (c) As(V) and P(V), and (d) As(III) and P(V).

As(III) binding the most, the effect is weaker than for As(V). Thus, these groups give rise to the strongest As(V) preference of -0.15, -0.17, -0.26, and -0.42 eV, respectively, shown in Figure 3b. The weaker H-bonding of As(III) compared to As(V) can be further seen in O···H bond lengths, which are 0.2, 0.1, 0.13, and 0.2 Å longer in Fc-R-As(III) than the Fc-R-As(V) bonds for the NH₂, NO₂, OH, and COOH substitutions, respectively. Conversely, the SH, C₂H₅, CH₃, and Cl substitutions only slightly influence the binding energies of both As(III) and As(V) and thus do not alter anion selectivity, providing at most a -0.07 eV As(V) preference, which lies within the error of the DFT method. Although As(III) binds via a similar mechanism to Fc-R as As(V), EDA reveals that the overall polarization and dispersion components of the interaction energies are more favorable for As(V) binding (mean values of -78.31 kcal/mol and -7.31 kcal/mol, respectively) than for As(III) (mean values of -23.76 kcal/mol and -4.8 kcal/mol, respectively), as shown in Table S2-S5. We attribute the stronger dispersion and polarization to the charged nature of the As(V) molecule (-1 e molecular charge) compared to the charge-neutral As(III).

P(V) binds more strongly with substituted Fc than neat Fc, paralleling the As(V) behavior. However, there is essentially no preference for As(V) over P(V) on substituted Fc, with only the Cl and OH functional groups giving rise to a meager -0.05and -0.06 eV binding energy difference, respectively, as shown in Figure 3c. The nearly equal binding energies of As(V) and P(V) mirror the nearly equal bond distances for Fc-R-As(V) and Fc-R-P(V); with differences of only 0.01 and 0.04 Å for the OH and Cl substitutions, respectively. We attribute the minimal binding energy differences between As(V) and P(V) to the high degree of similarity in molecular charges $(-1 e^{-})$ and net atomic charges between their O atoms, a difference of only 0.05 e-, which causes them to experience equivalent electrostatic and dispersion forces from Fc. Overall, these findings suggest that strong interaction between the Fc and binding oxyanions does not induce selectivity between the identical As(V) and P(V).

As P(V) and As(V) have very similar binding energetics, it directly follows that Fc-R selectively binds P(V) over As(III). Our calculations reveal that the preference for P(V) binding over As(III) is exacerbated by substitution with the functional groups, with binding energy differences up to 0.42 eV, as Figure 3d shows. Compared to the neat Fc molecule, which had no energetic preference for P(V) over As(III), COOH increased the preference for P(V) the most. In contrast, the SH, Cl, CH₃, and C₂H₅ groups had no impact. The preference for P(V) over As(III) can be explained with the same reasons as in the case of As(V) over As(III), i.e., dispersion forces and polarization favor the negatively charged P(V) molecule compared to the charge-neutral As(III), shown in Tables S2-S5. Based on our calculations, it is expected that P(V)would inhibit As(III) adsorption on substituted Fc more than As(V) adsorption.

3.4. As(V) Binding to Ferrocenium. Fc oxidizes to Fc⁺ through the removal of an electron from the Fe ion, which then adopts a 3+ state. In Fc⁺, one Cp ring relaxes to the side, forming a bent structure, shown in Figure 4a, because of weakened Fe-Cp covalent bonds. At their furthest, the Cp rings are 4.22 Å apart, a 24% increase over the ring separation distance in neutral Fc; thus, the bent structure exposes the Fe³⁺ metal center to possible attack by the oxyanions because of the substantially reduced steric hindrance with the Cp groups. We attribute the structural distortion of Fc⁺ to the Jahn–Teller effect, which breaks the orbital degeneracies near the highest occupied molecular orbital (HOMO) of the Fc⁺ molecule and lowers its total energy by -3.44 eV from the parallel Fc⁺ configuration. The bent structure is in agreement with previous findings. 65,66

Additionally, we find that upon oxidation Fc⁺ spontaneously relaxes to the bent structure, suggesting that this transformation has no kinetic limitations. Thus, the energetic gain in having nondegenerate orbitals in the bent structure outweighs the cost of Fe–C bond elongation per the Jahn–Teller effect. The observed distortion in the compact structure of Fc upon oxidation is consistent with the swelling behavior observed experimentally upon oxidation. ^{36,43,47}

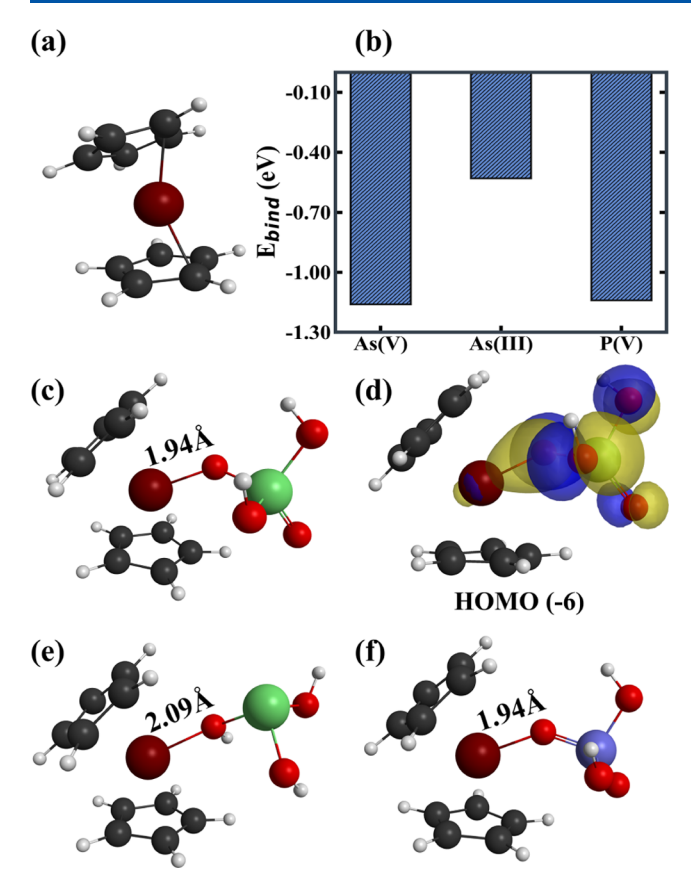


Figure 4. (a) Optimized Fc^+ showing its bent structure. (b) Oxyanion binding energies on neat Fc^+ . (c) Optimized structure for Fc^+ -As(V). (d) HOMO (-6) for Fc^+ -As(V). Optimized structures for (e) Fc^+ -As(III) and (f) Fc^+ -P(V). White spheres are hydrogens, black spheres are carbon, red spheres are oxygen, purple spheres are phosphorus, dark red spheres are iron, and green spheres are arsenic.

The binding behavior of As(V) to Fc⁺ differs from that to neutral Fc. The As(V) bond to Fc⁺ is almost 6 times stronger, -1.16 eV (as shown in Figure 4b), than to Fc, -0.19 eV, in agreement with the experimental finding that As(V) binds to Fc decorated electrodes more strongly under positive bias.³ The increased binding strength is due to increased coulombic attraction between the negatively charged As(V) and the positively charged Fc+ (see Table 1) and the formation of a covalent bond between an O atom of As(V) and Fe3+. This bond can form due to the decreased steric hindrance between As(V) O atom and the Cp rings. The resulting Fe-O bond length is only 1.94 Å, as shown in Figure 4c, within the range of reported Fe-O covalent bond lengths, ca. 1.75–2.07 Å, in α -Fe₂O₃.⁶⁷ The covalent bond is shown in Figure 4d. The bond formation is accompanied by a 0.33 e charge transfer from As(V) to Fc⁺, shown in Figure 5a, where the As atom contributes ~0.1 e and the binding O atom contributes the remaining ~0.2 e-. The electron density donated by the O atom forms a p-d σ -bond with the Fe. Concomitantly, Fe back-donates electron destiny, partially filling the As-O π^* antibond. This back-donation elongates the As-O bond by 0.05 Å to 1.70 Å and stabilizes the complex by 8.56 kcal/mol as determined via NBO and shown in Figure 5b.

3.5. As(III) and P(V) Binding to Ferrocenium. Oxidized Fc^+ also increases the binding energy of As(III) and P(V). Although As(III) binds to Fc^+ more strongly (-0.53 eV) than to Fc, it is 0.63 eV weaker than As(V). The weaker binding of

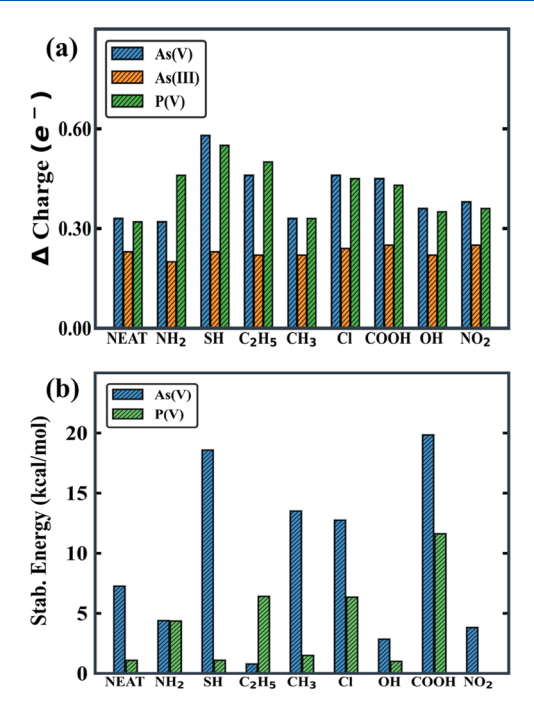


Figure 5. (a) Plot of changes in oxyanion natural charges upon binding to neat and substituted Fc^+ for As(V), As(III), and P(V), respectively. (b) Back-donation stabilization energies for the Fe-O bond obtained from NBO analysis for As(V) and P(V) bound to neat and substituted Fc^+ . More positive stabilization energy values correspond to stronger bond stabilization, i.e., higher back-donation.

As(III) is due to the decreased charge (0.23 e^-) transferred to Fe³⁺ (shown in Figure 5a), as well as weaker electrostatic and dispersion interactions, as shown in Table 1. This charge transfer difference arises from the higher energy of the As(V) HOMO, -137.42 kcal/mol, than As(III), -171.94 kcal/mol.

Unsurprisingly, P(V) behaves more similarly to As(V) than As(III). P(V) binds exothermically with a binding energy of -1.14 eV, which is only 0.02 eV weaker than As(V). There is no significant difference in the amount of charge transfer upon binding between As(V) and P(V), only 0.01 e⁻, which explains the similarity in binding energies between both oxyanions. The similar Fe-O bond strengths and mechanisms between Fc+-As(V) and Fc^+ -P(V) also result in equal bond lengths, 1.94 Å, respectively. We note, however, a slight difference in the π acceptor strengths of the oxyanions. NBO analysis of the orbital interactions reveals stronger charge delocalization, i.e., higher back-donation stabilization energies, from Fe orbitals to the O-As/P π^* orbitals for As(V) than for P(V), as shown in Figure 5b. Overall, we predict neat Fc⁺ to equally bind As(V) and P(V), and both interact more strongly with Fc+ than As(III).

3.6. Oxyanion Binding to Substituted Ferrocenium. Functional substitutions have varying effects on the core Fc^+ molecule. While COOH, OH, C_2H_5 , CH_3 , Cl, and NO_2 groups withdraw charge from Fc^+ , NH_2 and SH substitutions slightly donate charge (0.04 e⁻) as shown in Figure S4. All substituted Fc^+ -R molecules adopt similar distorted structures to the neat Fc^+ and are shown in Figure S8.

As in the nonoxidized Fc case, the H-bond donating groups, NH₂, OH, COOH, and NO₂, strengthen As(V) binding by 0.11 to 0.29 eV over neat Fc⁺, while SH, C₂H₅, CH₃, and Cl, weaken As(V) binding with binding energies from -1 to -1.45 eV, as shown in Figure 6a. As(V) binds via direct covalent

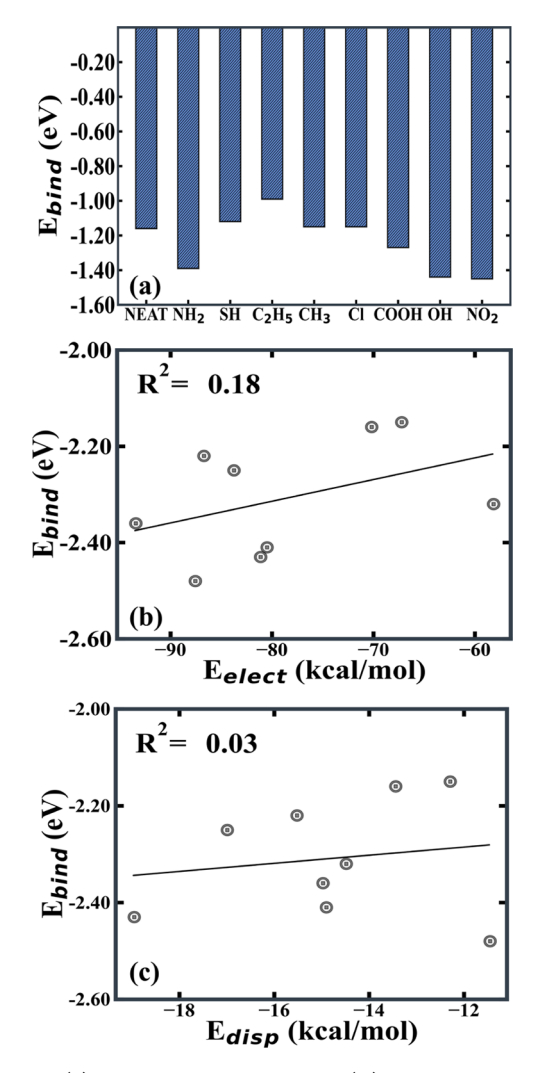


Figure 6. (a) Binding energies for As(V) bound to neat and substituted Fc^+ . Linear correlation plots of binding energy vs (b) electrostatic component and (c) dispersion component of the interaction between As(V) and Fc^+ .

bond formation with the Fe³⁺ center for all of the Fc⁺-R systems, like the neat Fc⁺ system. The covalent Fe-O bonds in the Fc⁺-R-As(V) molecules are 1.95, 2.08, 2.03, 1.95, 1.97, 1.93, 2.05, and 1.86 Å for the NH₂, SH, C₂H₅, CH₃, Cl, OH, COOH, and NO₂ substitutions, respectively, and their respective optimized structures are shown in Figure S9. Binding energies correlate poorly with the electrostatic and dispersion components of interaction energy, seen in Figure 6b,c, highlighting the fact that those forces no longer control oxyanion binding; rather the covalent bonding dominates.

The combination of the charged Fc^+ and substitutional groups induces a difference in binding energies among the oxyanions, where As(V) is slightly stronger than P(V), which are both much stronger than As(III). As in the case of neat Fc^+ , As(III) binding strength is 0.46-0.9 eV lower than As(V) for all substituted structures, achieving binding energies of -0.45 to -0.69 eV, as shown in Figure 7a. Further, the binding energy differences between As(III) and both As(V) and P(V), are up to 0.9 and 0.83 eV, respectively, which suggests a strong preference for both As(V) and P(V) over As(III), as shown in Figure 7b,c. As was highlighted before, As(III) forms a weaker

bond to Fc⁺-R due to lower charge transfer, and the side groups form weaker H-bonds to As(III).

The combination of charged Fc⁺ and substitutions induces the first appreciable binding energy difference between As(V) and P(V). NH2 and SH substitutions to Fc+ increase the energetic preference of As(V) over P(V) by -0.23 and -0.13eV, respectively, while OH, COOH, CH₃, C₂H₅, NO₂, and Cl substitutions show no significant oxyanion preference. The trend in preference for As(V) (seen in Figure 7d) is in good agreement with the trend in charge transfer effects of the functional groups on Fc⁺ (seen in Figure S4), where chargedonating groups induce a preference for As(V) over P(V). Thus, even though the Fc+-NO2 molecule achieved the strongest As(V) and P(V) binding, -1.45 and -1.42 eV, respectively, we predict that the NO2 group is ineffective for As(V) removal in P(V) competitive water matrixes because of the weak As(V) preference. Taken together, the best performance, i.e., binding strength and selectivity, is achieved with a charge and H-bond donating NH2 substitution, which results in -1.39 eV total binding energy of As(V) and a -0.23eV preference over P(V). Given this energetic preference, we predict Fc⁺-NH₂ to remove As(V) even when P(V) concentrations are ~270 times higher, based on the binding free energy and the Boltzmann distribution at room temperature. This result is consistent with the findings of Chen et al., where the metallopolymer, poly(ferrocenyldimethylsilane) (PFS) containing charge-donating silane groups achieved better selective As(V) removal over other similarly shaped transition-metal oxyanions than neat PVF under an applied potential of 0.8 V vs Ag/AgCl.34

Only the C_2H_5 group exhibits a preference for P(V) over As(V). Here, P(V) and As(V) bind to $Fc^+-C_2H_5$ in a bidentate configuration, whereas they bind in a monodentate configuration for the other substitutions. This finding suggests that a bidentate binding configuration favors P(V) over As(V). Additionally, NBO analysis reveals a more robust stabilization of the Fe-O bond when P(V) is bound to $Fc^+-C_2H_5$ than As(V). The stabilization energies for the Fe-O bond between Fc^+ and As(V)/P(V) are shown in Figure 5b. Overall, the combined oxidation of Fc to Fc^+ and substitution with charge and H-bond donating functional groups provides a route to the selective separation of As(V) over P(V) although preferential removal of the As(III) species over P(V) is unlikely with the Fc/Fc^+ system.

3.7. Protonation Effects on Oxyanion Binding to Ferrocene. To understand the role of oxyanion protonation extents, and thus system pH, on their binding affinity and selectivity to Fc and Fc-R, we calculated the binding energies of As(V), As(III), and P(V) to neat Fc and Fc-OH in their neutral states as a function of oxyanion protonation extent, i.e., fully protonated (H_3XO_y) , di-protonated $(H_2XO_y^{-})$, monoprotonated (HXO_y^{2-}) and deprotonated (XO_y^{3-}) where X represents As or P, while y represents the number of O atoms (4 for As(V) and P(V), respectively, and 3 for As(III)). The Fc-OH structure was chosen as the representative substituted Fc because it demonstrated the strongest binding while providing some selectivity toward As(V).

We predict that binding strength decreases monotonically with decreasing As(V) protonation on neat Fc; the fully protonated state binds exothermically by only -0.20 eV, while in the deprotonated state, it is endothermic by 0.11 eV, as shown in Figure 8a. P(V) behaves nearly identically to As(V); however, As(V) binding is slightly more exothermic than P(V)

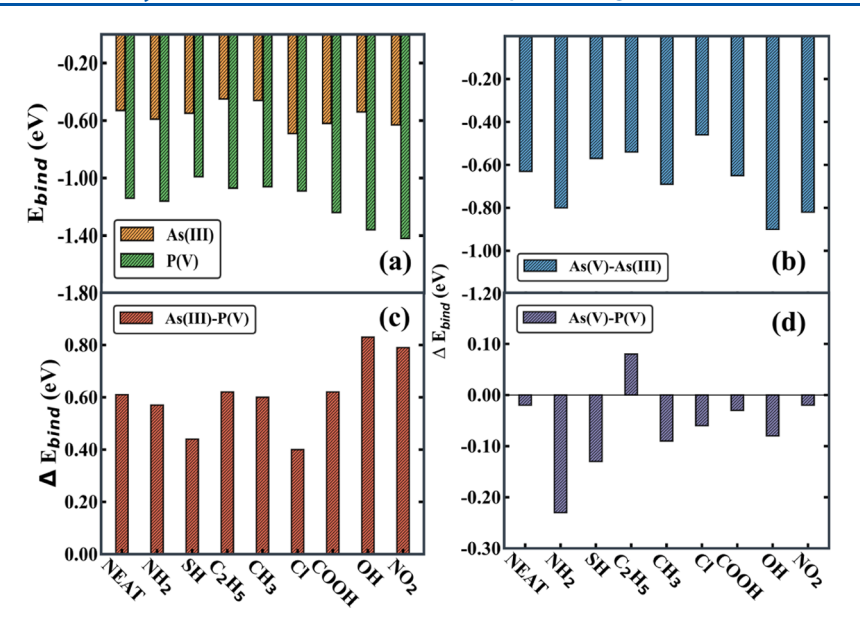


Figure 7. (a) Binding energies for As(III) and P(V) bound to neat and substituted Fc^+ . Binding energy differences when bound to Fc^+ between (b) As(V) and As(III), (c) As(III) and P(V), and (d) As(V) and P(V).

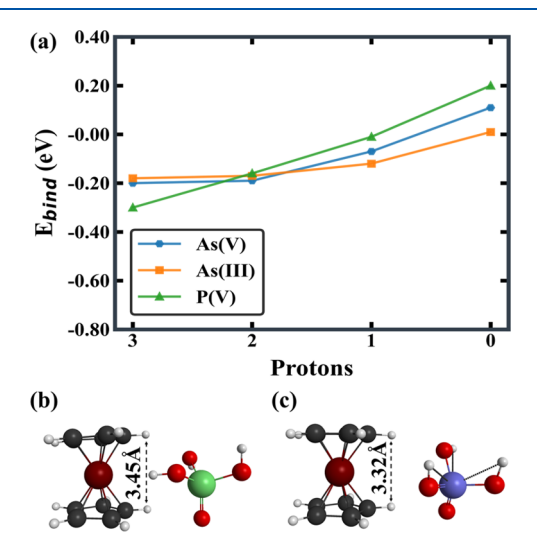


Figure 8. (a) Binding energies vs no. of protons for As(V), As(III), and P(V) bound to Fc (from fully protonated H_3XO_y) to deprotonated XO_y^{3-} . Optimized structures for (b) Fc-H₃AsO₄ and (c) Fc-H₃PO₄.

at all but the fully protonated state where P(V) is favored by 0.1 eV. In the fully protonated state, As(V) binds with an Hatom pointing toward the Cp rings, expanding the Fc structure. The resulting Cp ring distance is increased to 3.45 Å, as seen in Figure 8b. In contrast, fully protonated P(V) binds with its Hatoms pointing away from the Fc Cp rings; hence, the sandwich structure is less perturbed, with a Cp ring distance of 3.32 Å, shown in Figure 8c. The smaller structural distortion results in a more favorable binding of P(V) over As(V). We attribute the decreasing binding strengths with decreasing protonation extent to the increased electrostatic repulsion between the negatively charged oxyanions and the negatively charged Fc Cp rings.

While As(III) also shows a monotonic trend in binding strength similar to those of As(V) and P(V), it is preferred over both species in the mono-protonated state by up to -0.11 eV. The preference for As(III) occurs in a protonation state

that is very unlikely given the pK_a of As(III) (9.2) relative to both As(V) and P(V), 6.9 and 7.2, respectively. Thus, we expect all three oxyanions to adhere nearly equally and in small amounts to Fc in environmental conditions.

The presence of the OH functional group reverses the correlation between protonation extent and binding energy of neat Fc. When OH is present, oxyanion binding strength increases monotonically with decreasing protonation extent for As(V), As(III), and P(V), respectively, as shown in Figure S10. We attribute this difference in binding energy trend compared to the neat Fc case to the partial positive charge induced on the Fc molecule by substitutions (seen in Figure S4), which increases electrostatic attraction with more negatively charged oxyanions. This behavior is confirmed by the observation of a similar trend in binding energy with protonation extent calculated for the COOH substitution, which also withdraws charge from Fc, thus highlighting the influence of the substitutions in directing protonation-dependent oxyanion binding to Fc (see Figure S10). As was shown previously, although Fc-OH induces strong binding of As(V) and P(V) across protonation extents, it minimizes the energetic preference between them.

Conversely, As(III) binds more strongly than As(V) and P(V) in the mono-protonated and the deprotonated states (up to -0.42 and -0.4 eV stronger at both states, respectively), while it binds equally as both oxyanions in the di- and fully protonated state. When all three oxyanions bind to Fc-OH in the mono- and deprotonated states, there is a proton transfer from the OH group to the oxyanion. The proton transfer favors As(III) over both As(V) and P(V) and suggests that As(III) is a stronger Lewis base than the latter pair based on the energetics. We also calculate only a slightly higher mean charge density on the As(III) O atoms (-1.41 e⁻) compared to As(V) and P(V), -1.36 e-, which suggests that small electronic differences can significantly influence oxyanion proton transfer behaviors. We therefore expect that just like neat Fc, Fc-OH would exhibit no selective As removal at environmental conditions.

3.8. Protonation Effects on Oxyanion Binding to Ferrocenium. Similar calculations for binding the different oxyanion protonation states were done for neat Fc^+ , Fc^+ -OH, and Fc^+ -NH₂. The Fc^+ -OH and Fc^+ -NH₂ molecules were chosen since they achieved the strongest and most selective As(V) binding, respectively. We calculate that binding strength increases monotonically with decreasing protonation extent for As(V) bound to neat Fc^+ . The fully protonated state binds exothermically by only -0.22 eV, while the deprotonated state binds by -3 eV, as shown in Figure 9a. We attribute this trend to ionic attraction; with fewer protons, the more negatively charged species form a stronger bond than the neutral species.

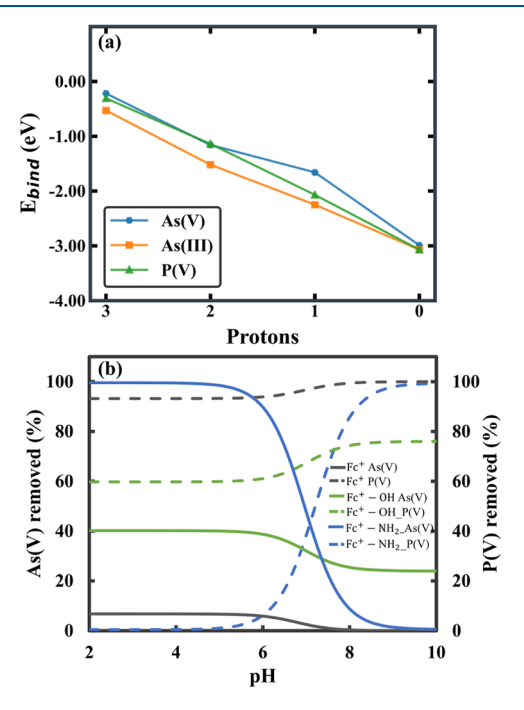


Figure 9. (a) Binding energies vs no. of protons for As(V), As(III), and P(V) bound to Fc^+ . (b) Predicted % As(V) and P(V) removed as a function of pH with equal oxyanion concentrations for Fc^+ , Fc^+ -OH, and Fc^+ -NH₂. Solid lines are for As(V), while dashed lines are for P(V).

P(V) and As(V) bind equally to Fc^{+} at all protonation extents except the mono-protonated state. P(V) is preferred by 0.42 eV in the mono-protonated state. The difference arises from the binding configuration, where mono-protonated P(V) binds in a bidentate configuration with a bond length of 2.03 Å while As(V) binds in a monodentate configuration with a bond length of 2.65 Å. This observation is consistent with the previously noted configuration effects for the $Fc^{+}\text{-}C_{2}H_{5}$ system, where bidentate binding configurations favored P(V) over As(V).

As(III) also follows a similar monotonic trend in binding energy; however, it is calculated to be preferred over both As(V) and P(V) at all but the deprotonated state where we predict equal binding for all three oxyanions (up to -0.31, -0.38, and -0.59 eV more favored at the fully, di, and monoprotonated states, respectively). These results suggest that P(V) would significantly impact As(V) adsorption on neat Fc⁺ across a wide range of pH conditions. Similarly, As(III) removal would also be hindered by P(V) because of the differences in their p K_a 's, which favor P(V) adsorption at environmental conditions.

Using our calculated binding energies, we predicted As(V) or P(V) uptake of Fc⁺ as a function of pH assuming that there is an excess of anions compared to the binding sites and an equal concentration of As(V) and P(V). As(III) was neglected because of the strong preference for As(V) and P(V) over As(III) in environmental conditions. The predicted oxyanion removal amounts are shown in Figure 9b. The As(V)/P(V)preference is characterized by three regimes: (1) pH < 6, where the deprotonated states dominate, (2) pH between 6 and 8, where there is a transition in protonation extent, and (3) pH \geq 8, where the mono-protonated state dominates. In Regime 1, only the di-protonated state is present; thus, the competition between the As(V) and P(V) is directly calculated via eq 5. Under these conditions, approximately 90% of the Fc⁺ sites are occupied by P(V) due to the more favorable binding free energies for P(V) than for As(V), shown in Figure S11. Regime 2 is more complex as multiple species of each ion may be present; this complexity is exacerbated by the large difference in binding free energies at different protonation extents, and thus highly different binding equilibrium constants. Hence, regime 2 is characterized by a steady decrease in As(V) uptake up with increasing concentration of the mono-protonated species until elevated pH ≥ 8 (regime 3), where the mono-protonated state dominates, and the much larger difference in free energies between P(V) and As(V) drives complete occupation by P(V).

The oxyanion protonation state influences its binding to Fc⁺-OH similarly to neat Fc⁺. While all three oxyanions bind increasingly strongly with decreasing protonation extent, As(V) and P(V) are essentially indistinguishable at all protonation states. As(III), on the other hand, is favored over both As(V) and P(V) (up to -0.54, -0.94, and -0.77 eV more favored at the di-, mono-, and deprotonated states, respectively) except in the fully protonated state where all three oxyanions bind equally, as shown in Figure S10. Just like the Fc-OH discussed previously, As(III) is favored over As(V) and P(V) in the mono- and deprotonated states due to its more favorable proton transfer compared to the latter pair. We predict that ~40% of As(V) is removed by Fc⁺-OH at low pH < 6 (regime 1). While above pH 6, P(V) increasingly dominates (Regime 2), resulting in decreased As(V) removal down to only $\sim 25\%$ at about pH ≥ 8 (Regime 3), as shown in Figure 9b.

Fc⁺-NH₂ only preferentially binds As(V) over P(V) in the di-protonated state (where it is -0.23 eV more favored) while they are indistinguishable at all other protonation states, as shown in Figure 10a. P(V) transfers more charge to Fc⁺ than As(V) in the di-protonated state while both oxyanions transfer equal amounts at all other protonation states, as shown in Figure 10b. Hence, we attribute the preference for As(V) over P(V) in the di-protonated state to simultaneously repulsive oxyanion and NH₂ charge effects on Fc⁺ which weakened the Fc⁺-NH₂-P(V) bond compared to As(V) causing it to be 0.22 Å longer. We predict ~100% preference for As(V) removal from aqueous solutions with an equal concentration of background P(V) at low pH (\sim 2 < pH < 6, Regime 1). The high selectivity steadily decreases to ~50% at pH ~7 (Regime 2) and finally approaches zero at pH \sim 9 (Regime 3), see Figure 9b.

As in the other cases, As(III) binds more strongly to Fc^+NH_2 than either As(V) and P(V) in the mono- and diprotonated states (up to -0.72 and -0.38 eV more strongly, respectively), while the latter pair are preferred in the fully

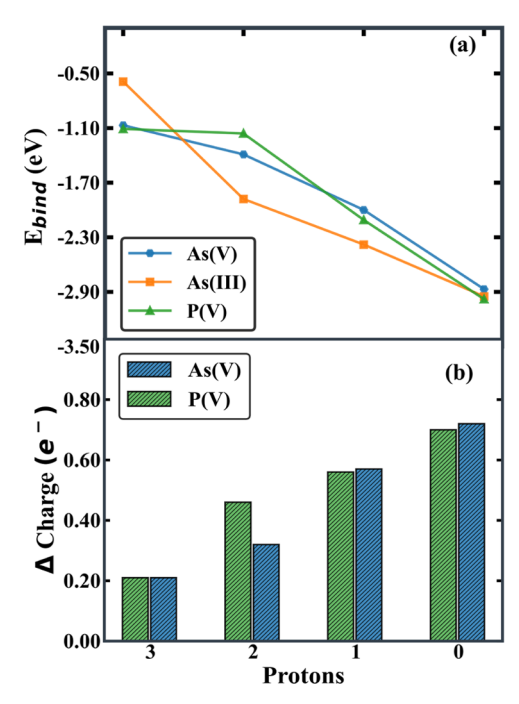


Figure 10. (a) Binding energies vs no. of protons for As(V), As(III), and P(V) bound to $Fc^+\text{-}NH_2$. (b) Plot of changes in oxyanion natural charges upon binding to $Fc^+\text{-}NH_2$ for As(V) and P(V) as a function of protonation extent.

protonated state. The difference in As(III) binding behavior between Fc⁺-OH and Fc⁺-NH₂, particularly at the deprotonated state, is due to the absence of proton transfer interactions in the Fc⁺-NH₂ system, which causes all three oxyanions to be equally bound. This is unlike the Fc⁺-OH system, where proton transfer interactions strongly favor As(III) over both As(V) and P(V). These findings suggest that preferential separation of As(V) over P(V) is only achievable by Fc⁺-NH₂ at pH conditions where they are diprotonated (2.3 < pH < 7), while, As(III) adsorption would be severely inhibited by P(V) across all pHs, due to oxyanion p K_a differences.

4. CONCLUSIONS

Using ab initio calculations, we have investigated the binding behavior of As(V), As(III), and P(V) on neat and substituted Fc and Fc^+ . We found that Fc cannot energetically discriminate between As(V), As(III), and P(V) because weak dispersion forces dominate the Fc-oxyanion interaction, thus making them indistinguishable. Oxidation of Fc to Fc^+ enables stronger binding of oxyanions because the oxidation distorts the otherwise stable sandwiched structure of Fc, allowing Fc^+ oxyanion covalent bonding. We calculate that neat Fc^+ binds As(V) and P(V) equally because they transfer equal amounts of charge to Fc^+ . However, both oxyanions bind more strongly to Fc^+ than As(III), which transfers significantly less charge to Fc^+ .

Functional group substitutions on Fc/Fc⁺ can improve oxyanion binding strengths and selectivity. Substitutions that donate charge to Fc⁺ and H-bond to oxyanion, particularly NH₂, are promising candidates for selectively binding As(V) over P(V). However, substitution is unable to induce a preference for As(III) relative to both As(V) and P(V) due to differences in oxyanion pK_a 's. We find a tradeoff between strong oxyanion binding and selectivity, especially for Fc⁺,

where strongly binding substitutions have smaller binding energy differences between the oxyanions. A broader sampling of functional groups may optimize the dual desire for strong and selective binding. Finally, the trend in total binding energies as a function of oxyanion protonation state suggests that operation in specific pH conditions may be necessary for the selective separation of As(V) over P(V). Specifically, the most selective Fc⁺-NH₂ molecule only prefers As(V) over P(V) when both oxyanions are in their di-protonated state, corresponding to 2.3 <pH <7. Overall, this work suggests that not only can the combination of redox and functional substitution be used in tandem to induce strong oxyanion adsorption and selectivity, where oxidation state changes drive oxyanion adsorption to Fc-containing compounds, while substitutional groups provide for fine-tuning of the behavior through changes to the electronic structure of the cyclopentadienyl groups, but also that the slight differences in protonation extents of P(V) and As(V) can be exploited.

ASSOCIATED CONTENT

5 Supporting Information

The Supporting Information is available free of charge at https://pubs.acs.org/doi/10.1021/acs.jpca.3c03826.

Binding energies and binding energy differences for As(V) bound to Fc using different basis sets; binding energies and binding energy differences for As(V) bound to Fc at different theory levels; changes in oxyanion charges upon binding to Fc/Fc-R; changes in Fc/Fc+ natural charge upon substitution and molecular model of Fc-R; optimized structures for Fc-R; optimized structures for As(V) bound to Fc-R; correlation of binding energy with components of the interaction energy; binding energies for each oxyanion at different binding sites; components of the interaction energy for oxyanions bound Fc/Fc+-R; optimized structures for Fc⁺-R; optimized structures for As(V) bound to Fc⁺-R; binding energies vs protons for oxyanions bound to Fc/ Fc+-R; binding free energies vs pH for Fc+-R; thermodynamic data for oxyanions; and predicted % As(V) and P(V) removed as a function of pH with different amounts of oxyanion solution entropy loss (PDF)

AUTHOR INFORMATION

Corresponding Author

Christopher Muhich — Chemical Engineering, School for the Engineering of Matter, Transport and Energy, Arizona State University, Tempe, Arizona 85287, United States; Materials Science & Engineering, School for the Engineering of Matter, Transport and Energy, Arizona State University, Tempe, Arizona 85287, United States; orcid.org/0000-0003-3089-559X; Phone: (480) 965-2673; Email: cmuhich@asu.edu

Authors

Obinna Nwokonkwo — Chemical Engineering, School for the Engineering of Matter, Transport and Energy, Arizona State University, Tempe, Arizona 85287, United States;
ocid.org/0009-0004-9862-3122

Vivienne Pelletier – Materials Science & Engineering, School for the Engineering of Matter, Transport and Energy, Arizona State University, Tempe, Arizona 85287, United States

Michael Broud – Materials Science and Engineering, University of Tennessee, Knoxville, Tennessee 37996, United States; orcid.org/0000-0002-4840-3488

Complete contact information is available at: https://pubs.acs.org/10.1021/acs.jpca.3c03826

Notes

The authors declare no competing financial interest.

ACKNOWLEDGMENTS

This work was supported by the National Institute of Environmental Health Sciences of the National Institutes of Health under Award Number P42ES030990 as part of the MEMCARE (Metals Mixtures: Cognitive Aging, Remediation, and Exposure Sources) project. This work was also partially supported by the Science and Technologies for Phosphorus Sustainability (STEPS) Center, a National Science Foundation Science and Technology Center (CBET-2019435). The content is solely the authors' responsibility and does not necessarily represent the official views of the National Institutes of Health or the National Science Foundation. In addition, the authors acknowledge support from Research Computing at Arizona State University for providing high-performance supercomputing services.

REFERENCES

- (1) Shaji, E.; Santosh, M.; Sarath, K. V.; Prakash, P.; Deepchand, V.; Divya, B. V. Arsenic contamination of groundwater: A global synopsis with focus on the Indian Peninsula. *Geoscience Frontiers* **2021**, *12*, 101079.
- (2) Ravenscroft, P.; Brammer, H.; Richards, K. Arsenic Pollution: A Global Synthesis; John Wiley & Sons, 2011.
- (3) Masindi, V.; Muedi, K. L. Environmental Contamination by Heavy Metals. In *Heavy Metals*, 2018.
- (4) Sun, G.; Yu, G.; Zhao, L.; Li, X.; Xu, Y.; Li, B.; Sun, D. Endemic Arsenic Poisoning. In *Endemic Disease in China*, Sun, D., Ed.; Springer: Singapore, 2019; pp 97–123.
- (5) Putila, J. J.; Guo, N. L. Association of arsenic exposure with lung cancer incidence rates in the United States. *PLoS One* **2011**, *6*, No. e25886.
- (6) Kumar, R.; Patel, M.; Singh, P.; Bundschuh, J.; Pittman, C. U., Jr.; Trakal, L.; Mohan, D. Emerging technologies for arsenic removal from drinking water in rural and peri-urban areas: Methods, experience from, and options for Latin America. *Sci. Total Environ.* 2019, 694, No. 133427.
- (7) Fendorf, S.; Michael, H. A.; van Geen, A. Spatial and Temporal Variations of Groundwater Arsenic in South and Southeast Asia. *Science* **2010**, 328, 1123–1127.
- (8) Terlecka, E. Arsenic Speciation Analysis in Water Samples: A Review of The Hyphenated Techniques. *Environ. Monit. Assess.* **2005**, 107, 259–284.
- (9) Xu, S.; Sabino, F. P.; Janotti, A.; Chase, D. B.; Sparks, D. L.; Rabolt, J. F. Unique Surface Enhanced Raman Scattering Substrate for the Study of Arsenic Speciation and Detection. *J. Phys. Chem. A* **2018**, 122, 9474–9482.
- (10) Smedley, P. L.; Kinniburgh, D. G. A review of the source, behaviour and distribution of arsenic in natural waters. *Appl. Geochem.* **2002**, *17*, 517–568.
- (11) Sarkar, A.; Paul, B. The global menace of arsenic and its conventional remediation A critical review. *Chemosphere* **2016**, *158*, 37–49.
- (12) Sharma, Y. C.; Srivastava, V.; Singh, V. K.; Kaul, S. N.; Weng, C. H. Nano-adsorbents for the removal of metallic pollutants from water and wastewater. *Environ. Technol.* **2009**, *30*, 583–609.
- (13) Banerji, T.; Kalawapudi, K.; Salana, S.; Vijay, R. Review of processes controlling arsenic retention and release in soils and

- sediments of Bengal basin and suitable iron based technologies for its removal. *Groundwater Sustainable Dev.* **2019**, *8*, 358–367.
- (14) Yamani, J. S.; Miller, S. M.; Spaulding, M. L.; Zimmerman, J. B. Enhanced arsenic removal using mixed metal oxide impregnated chitosan beads. *Water Res.* **2012**, *46*, 4427–4434.
- (15) Jain, C. K.; Singh, R. D. Technological options for the removal of arsenic with special reference to South East Asia. *J. Environ. Manage.* **2012**, *107*, 1–18.
- (16) Elimelech, M.; Phillip, W. A. The Future of Seawater Desalination: Energy, Technology, and the Environment. *Science* **2011**, 333, 712–717.
- (17) Nagarale, R. K.; Gohil, G. S.; Shahi, V. K. Recent developments on ion-exchange membranes and electro-membrane processes. *Adv. Colloid Interface Sci.* **2006**, *119*, 97–130.
- (18) Alka, S.; Shahir, S.; Ibrahim, N.; Ndejiko, M. J.; Vo, D.-V. N.; Manan, F. A. Arsenic removal technologies and future trends: A mini review. *J. Cleaner Prod.* **2021**, *278*, No. 123805.
- (19) Strathmann, H. Electrodialysis, a mature technology with a multitude of new applications. *Desalination* **2010**, *264*, 268–288.
- (20) Lata, S.; Samadder, S. R. Removal of arsenic from water using nano adsorbents and challenges: A review. *J. Environ. Manage.* **2016**, 166, 387–406.
- (21) Goldberg, S. Competitive Adsorption of Arsenate and Arsenite on Oxides and Clay Minerals. *Soil Sci. Soc. Am. J.* **2002**, *66*, 413–421.
- (22) Pincus, L. N.; Rudel, H. E.; Petrovic, P. V.; Gupta, S.; Westerhoff, P.; Muhich, C. L.; Zimmerman, J. B. Exploring the Mechanisms of Selectivity for Environmentally Significant Oxo-Anion Removal during Water Treatment: A Review of Common Competing Oxo-Anions and Tools for Quantifying Selective Adsorption. *Environ. Sci. Technol.* **2020**, *54*, 9769–9790.
- (23) Miller, S. M.; Spaulding, M. L.; Zimmerman, J. B. Optimization of capacity and kinetics for a novel bio-based arsenic sorbent, TiO2-impregnated chitosan bead. *Water Res.* **2011**, *45*, 5745–5754.
- (24) Miller, S. M.; Zimmerman, J. B. Novel, bio-based, photoactive arsenic sorbent: TiO2-impregnated chitosan bead. *Water Res.* **2010**, 44, 5722–5729.
- (25) Goldberg, S.; Johnston, C. T. Mechanisms of Arsenic Adsorption on Amorphous Oxides Evaluated Using Macroscopic Measurements, Vibrational Spectroscopy, and Surface Complexation Modeling. *J. Colloid Interface Sci.* **2001**, 234, 204–216.
- (26) Awual, M. R.; Jyo, A.; El-Safty, S. A.; Tamada, M.; Seko, N. A weak-base fibrous anion exchanger effective for rapid phosphate removal from water. *J. Hazard. Mater.* **2011**, *188*, 164–171.
- (27) Hawthorne, F. C. A bond-topological approach to theoretical mineralogy: crystal structure, chemical composition and chemical reactions. *Phys. Chem. Miner.* **2012**, *39*, 841–874.
- (28) Jain, A.; Loeppert, R. H. Effect of Competing Anions on the Adsorption of Arsenate and Arsenite by Ferrihydrite. *J. Environ. Qual.* **2000**, 29, 1422–1430.
- (29) Awual, M. R.; Hossain, M. A.; Shenashen, M.; Yaita, T.; Suzuki, S.; Jyo, A. Evaluating of arsenic (V) removal from water by weak-base anion exchange adsorbents. *Environ. Sci. Pollut. Res.* **2013**, *20*, 421–430
- (30) Zhang, X.; Zuo, K.; Zhang, X.; Zhang, C.; Liang, P. Selective ion separation by capacitive deionization (CDI) based technologies: a state-of-the-art review. *Environ. Sci.: Water Res. Technol.* **2020**, *6*, 243–257
- (31) Chen, R.; Sheehan, T.; Ng, J. L.; Brucks, M.; Su, X. Capacitive deionization and electrosorption for heavy metal removal. *Environ. Sci.: Water Res. Technol.* **2020**, *6*, 258–282.
- (32) Gamaethiralalage, J. G.; Singh, K.; Sahin, S.; Yoon, J.; Elimelech, M.; Suss, M.; Liang, P.; Biesheuvel, P.; Zornitta, R. L.; De Smet, L. Recent advances in ion selectivity with capacitive deionization. *Energy Environ. Sci.* **2021**, *14*, 1095–1120.
- (33) Suss, M. E.; Porada, S.; Sun, X.; Biesheuvel, P. M.; Yoon, J.; Presser, V. Water desalination via capacitive deionization: what is it and what can we expect from it? *Energy Environ. Sci.* **2015**, *8*, 2296–2319.

- (34) Chen, R.; Feng, J.; Jeon, J.; Sheehan, T.; Rüttiger, C.; Gallei, M.; Shukla, D.; Su, X. Structure and Potential-Dependent Selectivity in Redox-Metallopolymers: Electrochemically Mediated Multicomponent Metal Separations. *Adv. Funct. Mater.* **2021**, *31*, No. 2009307.
- (35) Su, X.; Hatton, T. A. Redox-electrodes for selective electrochemical separations. *Adv. Colloid Interface Sci.* **2017**, 244, 6–20.
- (36) Su, X.; Hatton, T. A. Electrosorption at functional interfaces: from molecular-level interactions to electrochemical cell design. *Phys. Chem. Chem. Phys.* **2017**, *19*, 23570–23584.
- (37) Su, X.; Kushima, A.; Halliday, C.; Zhou, J.; Li, J.; Hatton, T. A. Electrochemically-mediated selective capture of heavy metal chromium and arsenic oxyanions from water. *Nat. Commun.* **2018**, *9*, No. 4701
- (38) Su, X.; Kulik, H. J.; Jamison, T. F.; Hatton, T. A. Anion-Selective Redox Electrodes: Electrochemically Mediated Separation with Heterogeneous Organometallic Interfaces. *Adv. Funct. Mater.* **2016**, *26*, 3394–3404.
- (39) Hemmatifar, A.; Ozbek, N.; Halliday, C.; Hatton, T. A. Electrochemical Selective Recovery of Heavy Metal Vanadium Oxyanion from Continuously Flowing Aqueous Streams. *ChemSuschem* **2020**, *13*, 3865–3874.
- (40) Gómez Arrayás, R.; Adrio, J.; Carretero, J. C. Recent Applications of Chiral Ferrocene Ligands in Asymmetric Catalysis. *Angew. Chem., Int. Ed.* **2006**, *45*, 7674–7715.
- (41) Di Giannantonio, M.; Ayer, M. A.; Verde-Sesto, E.; Lattuada, M.; Weder, C.; Fromm, K. M. Triggered Metal Ion Release and Oxidation: Ferrocene as a Mechanophore in Polymers. *Angew. Chem., Int. Ed.* **2018**, *57*, 11445–11450.
- (42) Song, Z.; Garg, S.; Ma, J.; Waite, T. D. Selective Arsenic Removal from Groundwaters Using Redox-Active Polyvinylferrocene-Functionalized Electrodes: Role of Oxygen. *Environ. Sci. Technol.* **2020**, *54*, 12081–12091.
- (43) Otón, F.; Espinosa, A.; Tárraga, A.; de Arellano, C. R.; Molina, P. [3.3]Ferrocenophanes with Guanidine Bridging Units as Multisignalling Receptor Molecules for Selective Recognition of Anions, Cations, and Amino Acids. *Chem. Eur. J.* **2007**, *13*, 5742–5752.
- (44) Valério, C.; Fillaut, J.-L.; Ruiz, J.; Guittard, J.; Blais, J.-C.; Astruc, D. The Dendritic Effect in Molecular Recognition: Ferrocene Dendrimers and Their Use as Supramolecular Redox Sensors for the Recognition of Small Inorganic Anions. *J. Am. Chem. Soc.* **1997**, *119*, 2588–2589.
- (45) Ding, Y.; Zhao, Y.; Yu, G. A membrane-free ferrocene-based high-rate semiliquid battery. *Nano Lett.* **2015**, *15*, 4108–4113.
- (46) Kim, K.; Cotty, S.; Elbert, J.; Chen, R.; Hou, C.-H.; Su, X. Asymmetric Redox-Polymer Interfaces for Electrochemical Reactive Separations: Synergistic Capture and Conversion of Arsenic. *Adv. Mater.* **2020**, 32, No. 1906877.
- (47) Feng, X. F.; Yin, W. H.; Fan, Y. L.; Yin, M. J.; Xu, Z. Z.; Luo, F. General Approach for Constructing Mechanoresponsive and Redox-Active Metal—Organic and Covalent Organic Frameworks by Solid—Liquid Reaction: Ferrocene as the Versatile Function Unit. *Inorg. Chem.* **2020**, *59*, 5271—5275.
- (48) Gani, T. Z. H.; Ioannidis, E. I.; Kulik, H. J. Computational Discovery of Hydrogen Bond Design Rules for Electrochemical Ion Separation. *Chem. Mater.* **2016**, *28*, 6207–6218.
- (49) Youngran, J.; Fan, M.; Van Leeuwen, J.; Belczyk, J. F. Effect of competing solutes on arsenic(V) adsorption using iron and aluminum oxides. *J. Environ. Sci.* **2007**, *19*, 910–919.
- (50) Gaussian 16 RevA.03, 2016.
- (51) Bode, B. M.; Gordon, M. S. Macmolplt: a graphical user interface for GAMESS. J. Mol. Graphics Modell. 1998, 16, 133–138.
- (52) Becke, A. D. Density-functional thermochemistry. III. The role of exact exchange. *J. Chem. Phys.* **1993**, *98*, 5648–5652.
- (53) Stephens, P. J.; Devlin, F. J.; Chabalowski, C. F.; Frisch, M. J. Ab initio calculation of vibrational absorption and circular dichroism spectra using density functional force fields. *J. Phys. Chem. A* **1994**, *98*, 11623–11627.

- (54) Lee, C.; Yang, W.; Parr, R. G. Development of the Colle-Salvetti correlation-energy formula into a functional of the electron density. *Phys. Rev. B: Condens. Matter Mater. Phys.* **1988**, *37*, 785.
- (55) Grimme, S.; Antony, J.; Ehrlich, S.; Krieg, H. A consistent and accurate ab initio parametrization of density functional dispersion correction (DFT-D) for the 94 elements H-Pu. *J. Chem. Phys.* **2010**, 132. No. 154104.
- (56) Barone, V.; Cossi, M. Quantum Calculation of Molecular Energies and Energy Gradients in Solution by a Conductor Solvent Model. *J. Phys. Chem. A* **1998**, *102*, 1995–2001.
- (57) Cossi, M.; Rega, N.; Scalmani, G.; Barone, V. Energies, structures, and electronic properties of molecules in solution with the C-PCM solvation model. *J. Comput. Chem.* **2003**, *24*, 669–681.
- (58) Gupta, S.; Anh Nguyen, N.; Muhich, C. L. Surface water H-bonding network is key controller of selenate adsorption on [012] α -alumina: An Ab-initio study. *J. Colloid Interface Sci.* **2022**, *617*, 136–146
- (59) Foster, J. P.; Weinhold, F. Natural hybrid orbitals. *J. Am. Chem. Soc.* **1980**, *102*, 7211–7218.
- (60) Su, P.; Li, H. Energy decomposition analysis of covalent bonds and intermolecular interactions. *J. Chem. Phys.* **2009**, *131*, No. 014102.
- (61) Gordon, M. S.; Schmidt, M. W. Advances in Electronic Structure Theory: GAMESS a Decade Later. In *Theory and Applications of Computational Chemistry*, Dykstra, C. E.; Frenking, G.; Kim, K. S.; Scuseria, G. E., Eds.; Elsevier, 2005; Chapter 41, pp 1167–1189.
- (62) CRC Handbook of Chemistry and Physics. 84th Edition Edited by David R. Lide (National Institute of Standards and Technology). CRC Press LLC: Boca Raton. 2003. 2616 pp. ISBN 0-8493-0484-9. J. Am. Chem. Soc. 2004, 126, 1586.
- (63) Zhu, X.; Nordstrom, D. K.; McCleskey, R. B.; Wang, R. Ionic molal conductivities, activity coefficients, and dissociation constants of HAsO42— and H2AsO4— from 5 to 90 °C and ionic strengths from 0.001 up to 3molkg—1 and applications in natural systems. *Chem. Geol.* **2016**, 441, 177—190.
- (64) Hay, B. P.; Dixon, D. A.; Bryan, J. C.; Moyer, B. A. Crystallographic Evidence for Oxygen Acceptor Directionality in Oxyanion Hydrogen Bonds. *J. Am. Chem. Soc.* **2002**, *124*, 182–183.
- (65) Lauher, J. W.; Hoffmann, R. Structure and chemistry of bis (cyclopentadienyl)-MLn complexes. *J. Am. Chem. Soc.* **1976**, 98, 1729–1742.
- (66) Veiros, L. F. Haptotropic Shifts in Cyclopentadienyl Organometallic Complexes: Ring Folding vs Ring Slippage. *Organometallics* **2000**, *19*, 5549–5558.
- (67) Nguyen, M.-T.; Seriani, N.; Gebauer, R. Defective α -Fe2O3(0001): An ab Initio Study. *ChemPhysChem* **2014**, *15*, 2930–2935.